Materials Selection for Use in Concentrated Hydrochloric Acid

Ajit Mishra,[‡,] Dave Shoesmith,[**] and Paul Manning[*]*

ABSTRACT

Hydrochloric acid (HCl) is an important mineral acid with many uses, including the pickling of steel, acid treatment of oil wells, and chemical cleaning and processing. This acid is extremely corrosive and its aggressiveness can change drastically depending on its concentration, the temperature, and contamination by oxidizing impurities. One of the most commonly encountered oxidizing impurities is the ferric ion. In general, stainless steels cannot tolerate aggressive HCl solutions, hence the need to use corrosion resistant nickel-based alloys. A part of this study focused on the role of alloying elements on the corrosion performance of commercial nickel-based alloys UNS N10276, UNS N06022, UNS N06200, UNS N07022, UNS N10362, UNS N10675, UNS N06059, and UNS N06625, in HCl solutions, with and without the presence of oxidizing impurities (ferric ions). Aggressive HCl solutions can also be used to simulate the critical crevice solution. Therefore, another aspect of this research is to investigate the role of alloying elements in nickel-based alloys on the inhibition of crevice corrosion. In the present study, various standard corrosion test methodologies, conservative electrochemical techniques, and a range of surface analytical tools have been utilized.

KEY WORDS: auger electron spectroscopy, crevice corrosion, hydrochloric acid, nickel alloys, potentiodynamic, scanning electron microscopy, surface profilometer, x-ray photoelectron spectroscopy

INTRODUCTION

Hydrochloric acid (HCl) is an important mineral acid, second only to sulfuric acid (H_2SO_4) in its uses in industry.[1] Major applications include acid pickling of steel, acid treatment of oil wells, chemical cleaning and processing, ore reduction, production of chlorine and chlorides, and food processing. There is a very limited choice of materials for use in this solution, as most of the commonly used metals and their alloys experience extensive general and/or localized corrosion attack in the HCl. Further, the solution aggressiveness drastically changes depending upon the concentration, temperature, and the presence of oxidizing impurities (like ferric ions, cupric ions, etc.).

Nickel alloys containing optimum amounts of chromium (Cr), molybdenum (Mo), and tungsten (W) are widely used in the chemical process industries because of their tolerance to both oxidizing and reducing conditions.[2] Major alloying elements like Cr and Mo (or Mo + W) play an important role in maintaining the passivity of the alloy and stabilizing the passive film after a localized breakdown event.[3] Chromium forms the primary Cr_2O_3 passive film, which is dominantly responsible for passivation, while Mo (and W) is known to inhibit localized corrosion by oxide reformation within initiated pits, thereby retarding their growth.[4-7]

Meck, et al.,[8] studied the corrosion performance of UNS N10675[(1)] (Ni-Mo alloy) and UNS N06200 (Ni-Cr-Mo-Cu) alloys in reagent grade HCl acid, with and

Submitted for publication: July 15, 2016. Revised and accepted: August 15, 2016. Preprint available online: August 15, 2016, http://dx.doi.org/10.5006/2193.

[‡] Corresponding author: E-mail: ajitosu@gmail.com.
[*] Haynes International, 1020 W. Park Avenue, Kokomo, IN 46902.
[**] Department of Chemistry, Western University, London, ON N6A 5B7, Canada.

(1) UNS numbers are listed in *Metals and Alloys in the Unified Numbering System*, published by the Society of Automotive Engineers (SAE International) and cosponsored by ASTM International.

ISSN 0010-9312 (print), 1938-159X (online)
17/000013/$5.00+$0.50/0 © 2017, NACE International

without the presence of impurities, using an electrochemical technique. In the reagent grade HCl solution, UNS N10675 demonstrated a high corrosion resistance. However, in the presence of oxidizing impurity, the corrosion resistance of UNS N06200 was significantly higher compared to UNS N10675. The results are in consensus with the weight loss data.[2]

In this study, the role of alloying elements in a number of commercially available nickel-based alloys was evaluated in several aggressive environments using weight loss and electrochemical measurements in conjunction with the surface characterization techniques.

EXPERIMENTAL PROCEDURES

Corrosion tests were conducted on C-2000[(2),†] (UNS N06200), Alloy 59 (UNS N06059), C-22®,† (UNS N06022), C-22HS®,† (UNS N07022), HAYNES® 625† (UNS N06625), HASTELLOY® C-276† (UNS N10276), HYBRID-BC1®,† (UNS N10362), and B-3®,† (UNS N10675) alloys. The nominal compositions of the studied alloys are shown in Table 1.

Corrosion Tests

Immersion Technique — Corrosion tests of the wrought alloys were performed under laboratory conditions using glass flask/condenser systems and reagent grade chemicals. The sample dimensions were 25 × 25 × 3 mm. The surfaces of these samples were ground using 120 to 600 grit papers, then degreased with acetone, prior to weighing and then testing of the samples. A test duration of 96 h was selected, with interruptions every 24 h to weigh the samples. The solution used was concentrated HCl acid and the testing temperature was from 39°C to 93°C. Corrosion studies were also performed in HCl solutions to which various amounts of oxidizing impurity had been added. In the present study, because many experiments were performed, not all of the experiments were repeated. However, a few experiments were selected randomly and repeated to ensure that the results were reproducible.

Electrochemical Techniques — For electrochemical measurements, specimens with a total surface area of ~14 cm^2 were cut from the plate materials. A small tapped hole was machined in the top of the specimen to enable contact, via a cylindrical rod, to external circuitry. This rod was sheathed in glass and sealed with a polytetrafluoroethylene (PTFE) gasket to prevent contact with the electrolyte. The sample was then polished with a series of wet silicon carbide papers up to 600 grit, rinsed with deionized (DI) water and acetone, and then air dried prior to an experiment. A platinum (Pt) foil and a saturated calomel electrode (SCE) were used as the counter and reference electrode, respectively.

TABLE 1
Nominal Alloy Compositions (wt% of major alloying element)

Alloys	Cr	Mo	W	Cu	Ni
UNS N06200	23	16		1.6	Bal.
UNS N06059	23	16			Bal.
UNS N06022	22	13	3		Bal.
UNS N07022	21	17			Bal.
UNS N06625	21	9			Bal.
UNS N10276	16	16	4		Bal.
UNS N10362	15	22			Bal.
UNS N10675	1.5	28.5			Bal.

The electrochemical tests were performed in deaerated 20% HCl at various temperatures. The open-circuit potential (OCP) was recorded for 1 h to allow a near steady-state value to be approached. Subsequently, linear polarization resistance (LPR) measurements were conducted as per ASTM Standard G-59,[9] from –20 mV to 20 mV of the corrosion potential (E_{corr}). Potentiodynamic polarization (PP) tests were performed from –250 mV below E_{corr} to 1,100 mV above at a scan rate of 0.167 mV/s in the forward direction. To study the effects of impurities in HCl on the corrosion behavior, electrochemical experiments (OCP, LPR, and PP) were conducted in 20% HCl containing various concentrations of Fe^{3+} ions.

For the crevice corrosion study, two different crevice arrangements were used: (a) a multiple crevice assembly (MCA) and (b) a single crevice assembly (SCA). The experimental details and the electrochemical techniques utilized when using these arrangements have been reported elsewhere.[7,10-12] The electrolyte used for crevice corrosion experiments was 1 M NaCl. In SCA, the temperature selected was 105°C and a galvanostatic current of 20 μA was applied to guarantee crevice initiation and to control its propagation. In MCA experiments, the potentiodynamic-galvanostatic-potentiodynamic (PD-GS-PD) technique[7,11] was used at 80°C, as the primary goal of the experiments was to measure breakdown and repassivation potentials and critical temperatures.[7]

Characterization Techniques — Electrodes anodically oxidized for surface analyses were rinsed gently with DI water and air dried prior to characterization. X-ray photoelectron spectroscopy (XPS) analyses were performed with a Kratos Axis Ultra† XPS at Surface Science Western (SSW) using monochromatic Al K_α (1,486.8 eV) radiation. The binding energy was calibrated to give an Au $4f_{7/2}$ line position at 83.95 eV. XPS spectra were corrected for charging by taking the C1s spectrum for adventitious carbon to be at a binding energy of 284.8 eV. Survey spectra were recorded on all samples, followed by high-resolution XPS spectra for Ni2p, Cr2p, Mo3d, W4f, C1s, and O1s spectral regions. The scanning electron microscopy

(2) HASTELLOY®, HAYNES®, C-22®, C-2000®, HYBRID-BC1®, and B-3® are registered trademarks of Haynes International, Inc.
† Trade name.

(SEM) images of the creviced corroded specimens were obtained on a LEO 440† SEM equipped with an EDAX† energy-dispersive x-ray spectroscopy (EDX) system. The depth of penetration and images of the corroded region were obtained using surface profilometry.

On completion of a crevice corrosion experiment, the corroded electrode was removed from solution, rinsed with DI water to remove electrolyte, and immediately dried. Optical microscopy, SEM and EDX analyses, and auger electron spectrometer (AES) depth profiling were performed to investigate the topography and elemental compositions of the corroded areas. The depth of penetration and 3D images of the corroded region were obtained using surface profilometry.

Optical microscopy was performed with a Zeiss Axioplan Compound Microscope† and a WILD M3Z Stereomicroscope†. Surface topography was observed using a SEM equipped with an EDX system to determine the elemental composition of the surface. Profilometry was performed with a Tencor P-10† stylus profiler, a mechanical stylus surface profiler that measures the surface topographical features. The stylus was a diamond probe (~2 µm in radius) attached to a tungsten tip. The scan speed was 50 µm/s. A 3D topographic image of a corroded surface was obtained from a series of surface line scans.

Auger analyses were performed using a PHI 660† AES with an excitation energy of 5 keV. Depth profiles were obtained by sputtering with an Ar^+ ion beam. A survey scan was acquired for each sample and during depth profiling the signal intensities for Ni, Cr, Mo, and O were monitored as a function of sputtering time. To convert sputtering times to penetration depths, similar measurements were performed on a UNS N06059 specimen covered with an air-formed native oxide. The sputtering rate obtained on this reference specimen was 32 nm/min and it was assumed that a similar sputtering rate was achieved on a corroded surface.

RESULTS AND DISCUSSION

The corrosion rate (in mils per year), obtained from weight change measurements, in various concentrations of HCl acid are shown in Figure 1. The rates for UNS N10675 and N10362 are the lowest over a wide range of HCl concentrations. Based on their corrosion resistance performance in HCl at the studied temperatures, the alloys can be ranked (high to low) as:

$$N10675 > N10362 > N10276 > N06200 > N06022 \quad (1)$$

The ranking follows the same trend as the amount of Mo (or Mo + 0.5 W)[7] in the respective alloys, which decreases in the same sequence from UNS N10675 to the lowest, UNS N06022. It must be taken into consideration that even though both Mo and W behave similarly, Mo demonstrates a better corrosion resistance than W, in low pH reducing solutions, for a similar concentration (in wt%).[7] The effect of temperature on the corrosion rate in HCl was also investigated, as shown in Figure 2. As observed in Figure 1, the corrosion rate of UNS N10675 was the lowest across the whole temperature range. A 20 mpy (0.508 mm/y) line is included in Figure 2, as the corrosion rate above 20 mpy is generally considered high from the end users' perspective.

At higher temperatures (e.g., T > 60°C), where the solution aggressiveness increases significantly, the

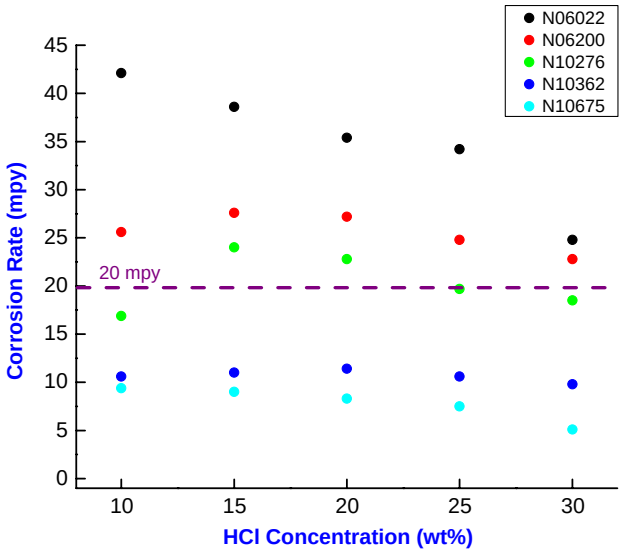

FIGURE 1. *Corrosion rates of a number of Ni-based alloys in HCl at 66°C obtained from weight change measurements.*

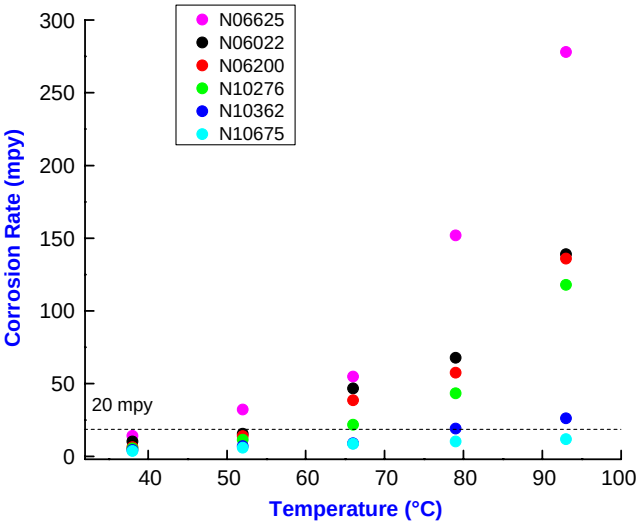

FIGURE 2. *Corrosion rates of a number of Ni-based alloys in 20 wt% HCl at various temperatures obtained from weight change measurements.*

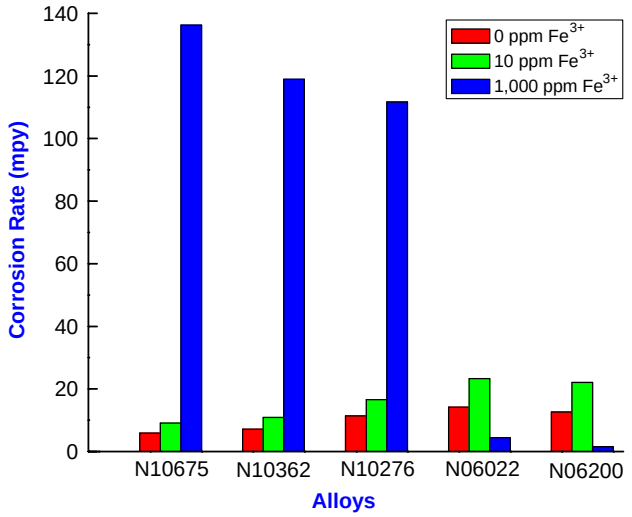

FIGURE 3. *Corrosion rates of various alloys in 20 wt% HCl acid, with and without added Fe^{3+}, at 52°C obtained from weight loss technique.*

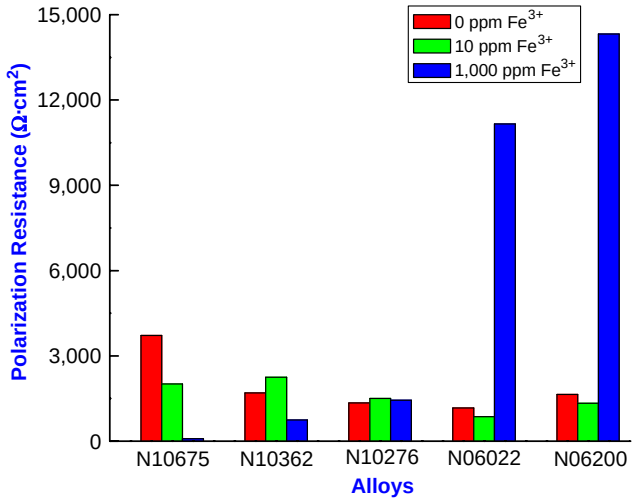

FIGURE 4. *Polarization resistance (R_p) of various alloys in 20 wt% HCl acid, with and without added Fe^{3+}, at room temperature.*

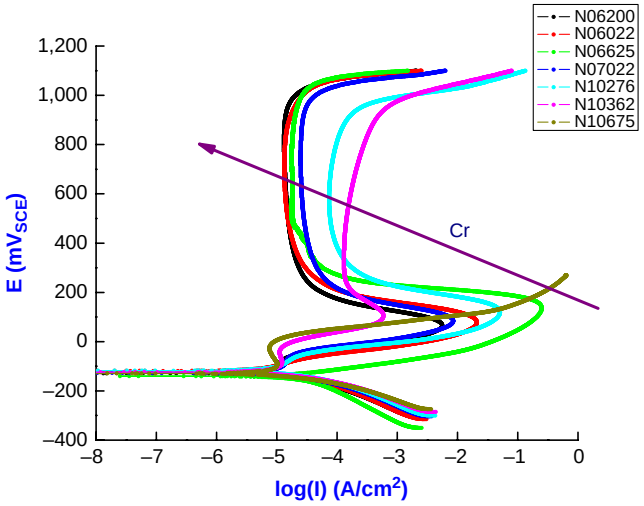

FIGURE 5. *Potentiodynamic polarization curves in 20 wt% HCl at an ambient temperature.*

corrosion rate is still low for UNS N10675 and N10362. Based on this corrosion data, UNS N10675 can be selected as the most corrosion resistant alloy, followed by UNS N10362 for application in reagent grade HCl.

As industrial HCl acid is not similar to reagent grade because of the presence of impurities (primarily Fe^{3+} ions) in the former, the role of Fe^{3+} on corrosion in HCl acid was investigated. Corrosion rates were obtained in 20% HCl at 52°C, with and without the presence of Fe^{3+} (Figure 3). In the absence, or when only a very small concentration (10 ppm) of Fe^{3+} was present in the HCl, the corrosion rate was lowest for UNS N10675 and highest for UNS N06022. However, when the concentration of Fe^{3+} was high (1,000 ppm), the corrosion rate was highest for UNS N10675 and lowest for UNS N06200.

The corrosion resistance performance of various corrosion resistant alloys can be ranked (high to low) as follows.

In 20% HCl at 52°C:

N10675 > N10362 > N10276 > N06200 > N06022 (2)

In 20% HCl + 10 ppm ferric ions at 52°C:

N10675 > N10362 > N10276 > N06200 > N06022 (3)

In 20% HCl + 1,000 ppm ferric ions at 52°C:

N06200 > N06022 > N10276 > N10362 > N10675 (4)

Based on the corrosion data in 20% HCl solution, with and without the addition of ferric ions (2 to 4), it can be concluded that a nickel-based alloy containing high Mo (UNS N10675 in the present study) will demonstrate the best corrosion resistance in HCl acid. However, in presence of high concentrations of impurity, an alloy containing high Cr (UNS N06200 in the present study, Table 1) will experience the lowest corrosion attack.

To better understand the corrosion mechanism, electrochemical tests were conducted in 20% HCl and 20% HCl + Fe^{3+} ions. The polarization resistance (R_p) values, determined using the LPR technique (Figure 4), show a similar trend in corrosion resistance performance of various alloys in 20% HCl acid (with and without the presence of Fe^{3+} ions) as observed from the weight loss measurements. The PP graphs (Figure 5) recorded in 20% HCl clearly show a strong relationship between alloys' Cr content and the passivation current density, with a high amount of Cr resulting in a low passivation current density (i_p). A low i_p can be attributed to the presence of a protective and less defective passive film. The PP study showed no passive

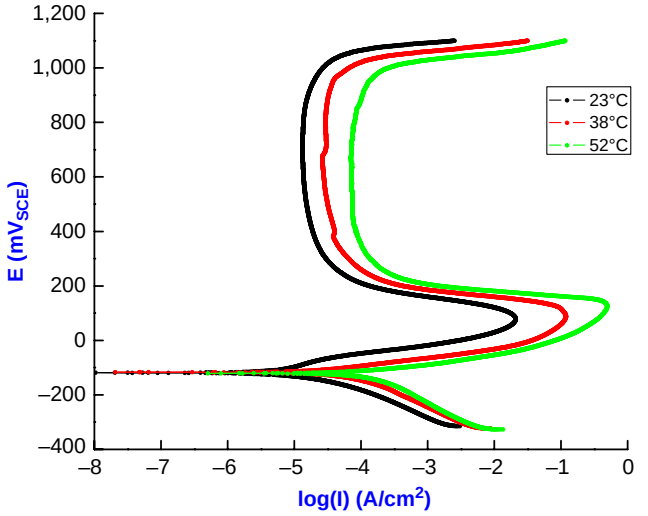

FIGURE 6. *Potentiodynamic polarization curves recorded on UNS N06022 in 20 wt% HCl at various temperatures.*

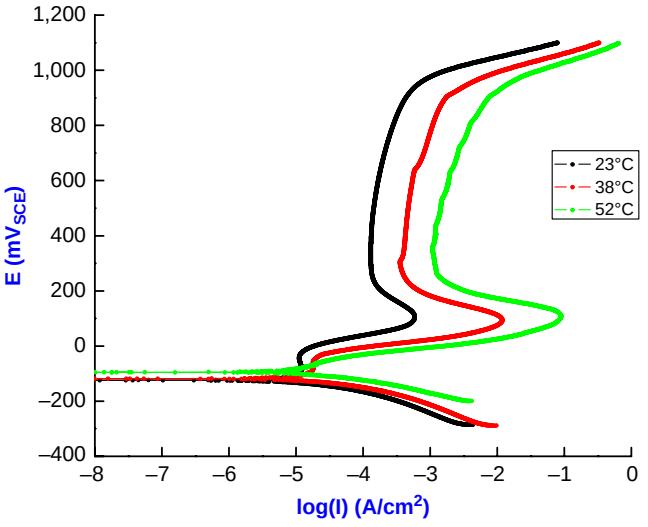

FIGURE 7. *Potentiodynamic polarization curves recorded on UNS N10362 in 20 wt% HCl at various temperatures.*

film was formed on UNS N10675 (Table 1). As Fe^{3+} is a strong oxidant, the absence of a passive film resulted in a high corrosion rate on UNS N10675 in 20% HCl + 1,000 ppm Fe^{3+} (Figure 3).

Electrochemical tests were also performed in HCl at various temperatures (Figures 6 and 7). With an increase in the temperature from ambient to 52°C, both the passivation current density (i_p) and the corrosion current density (i_{corr}) increase by almost an order of magnitude for UNS N06022 (Figure 6). As i_{corr} is directly proportional to the corrosion rate, this indicates an increase in corrosion rate with temperature for UNS N06022. However, in an identical environment for UNS N10362, i_p increases by more than an order of magnitude, while i_{corr} showed little change (Figure 7), in agreement with the weight loss data (Figures 1 and 2).

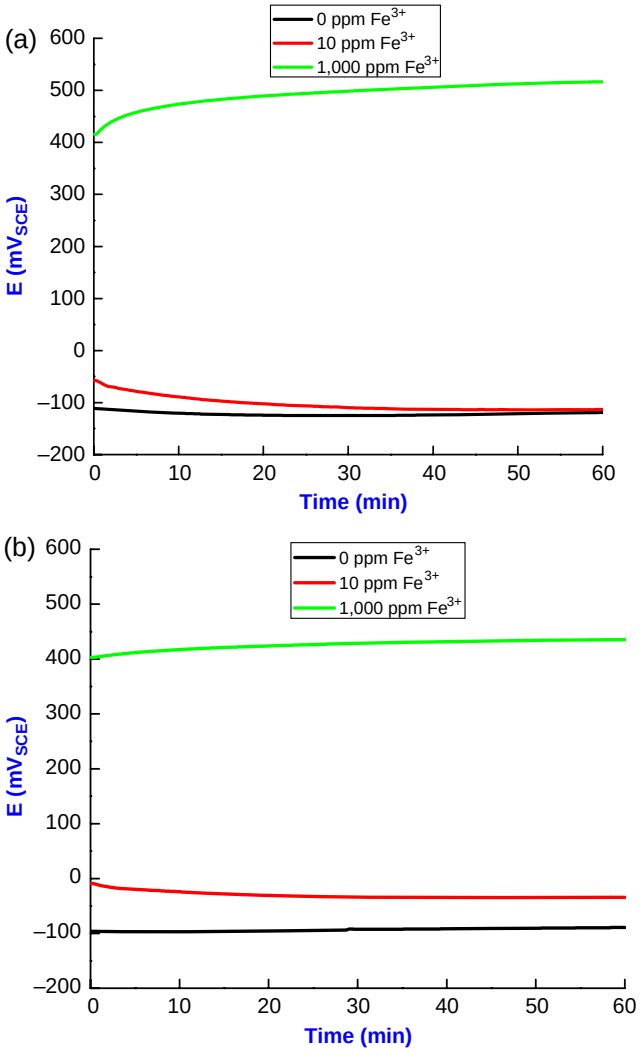

FIGURE 8. *OCP in 20 wt% HCl, with and without added Fe^{3+} impurity, at an ambient temperature for (a) UNS N06022 and (b) UNS N10362.*

This independence of corrosion rate on concentration and temperature for Mo-enriched alloys suggests the formation of a protective oxide film of Mo, which plays a major role in maintaining passivity. Based on these studies, the most suitable alloys for use in reagent grade concentrated HCl are UNS N10675 and N10362.

OCP curves recorded on UNS N06022 and N10362 in 20% HCl, with and without the presence of Fe^{3+}, are shown in Figure 8 and clearly demonstrate the oxidizing nature of Fe^{3+} ions. A schematic illustrating the role of oxidants (Fe^{3+}) on the corrosion performance of Ni-based alloys is shown in Figure 9. The figure includes two polarization curves, one for a low Mo (Mo + W)-high Cr alloy (black curve) and one for a high Mo (Mo + W)-low Cr alloy (red curve). A sufficient concentration of added Fe^{3+} (leading to the cathodic current potential relationship indicated by the blue line) will lead to an OCP in the passive region as indicated by the intersection of the blue line with the two

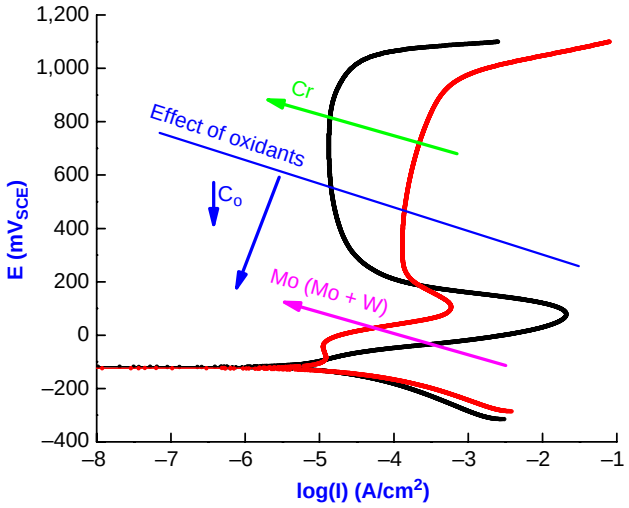

FIGURE 9. *Schematic of effect of oxidants on the corrosion performance of Ni-Cr-Mo (W) alloys.*

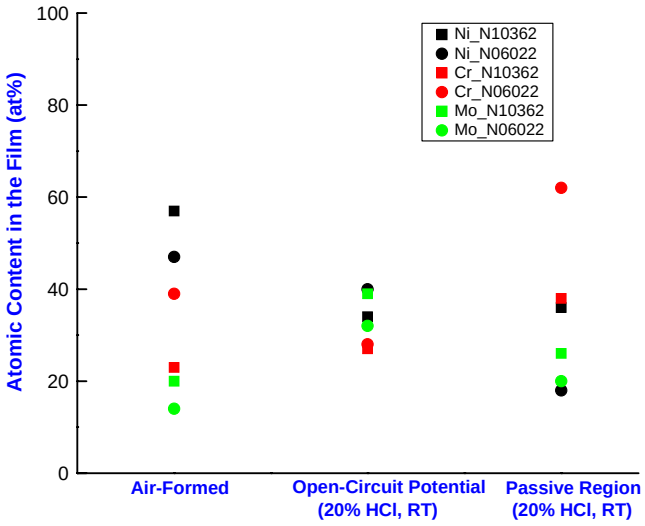

FIGURE 10. *Atomic concentration of major alloying elements obtained from XPS survey spectra.*

polarization curves. Under these conditions, the passive current (and hence the corrosion rate) would be lower on the high Cr alloy (indicated by the green arrow). However, if the Fe^{3+} concentration was less than the critical current density (the peak current during the active to passive transition), the blue line would eventually shift to lower potentials and into the active region as indicated by the blue arrows (with C_o indicating the decrease in oxidant concentration). Under these conditions, consistent with the present observations, the corrosion rate would be expected to decrease as the Mo (Mo + W) content of the alloy increased. The presence of ferric ions in HCl solution, or any aqueous solution, simply influences the overall cathodic reaction as a result of the reduction of ferric ions to a lower oxidation state. Thus, among Ni-Cr-Mo (W) alloys, an alloy having higher amount of Cr will demonstrate a better corrosion resistance in HCl solution containing moderate to high amount of ferric ions.

Another interesting observation in the PP curves in HCl solution is the anodic current behavior in the active region (i.e., between the corrosion potential and the active-passive transition) for alloys enriched in Mo (or Mo + W) (Figures 5 and 9). The current arrest at potentials lower than the active to passive transition indicates a distinct suppression of active dissolution as the Mo (Mo + W) content is increased, as observed in Figures 5 and 9.

XPS technique was used to analyze the composition of the oxide films formed at OCP (for 5 h) or potentiostatic polarization in the passive region (500 mV_{SCE}; hold time as 5 h) in 20% HCl. For comparison, the composition of the native oxide (i.e., that form by air exposure) was also determined. Figure 10 shows the atomic concentration (expressed as at% of cation content) obtained from XPS survey spectra.

In the air-formed film, the Cr is enriched as expected but the film is dominated by the Ni content on both alloys. In the passive region, both alloys are enriched in Cr and depleted in Ni, in particular the high Cr-containing UNS N06022, confirming that the low passive current density measured on this alloy (Figure 5) is a result of Cr enrichment. There is also a slight enrichment in Mo content, but this is slight considering the difference in Mo content in the two alloys. Under natural corrosion conditions the surface of both alloys is strongly depleted in Ni but enriched in Mo not Cr. This enrichment is slightly greater for the high Mo UNS N10362 than the lower Mo (+W) containing UNS N06022. Although the differences in Mo content on the surfaces of the two alloys are relatively small, this enhancement is consistent with the relative, small difference in corrosion rates between the two alloys measured by weight loss at low temperatures (Figure 2).

While Ni-Cr-Mo (W) alloys are generally not susceptible to pitting, crevice corrosion remains a possibility under sufficiently aggressive conditions.[7] To investigate the conditions that could apply under active crevice conditions, crevice corrosion was forced to initiate using an applied current of 20 μA. Figure 11 shows the potential-time curve recorded on UNS N06022 in 1 M NaCl at 105°C using the SCA. The initiation of crevice corrosion is indicated by the ~400 mV drop in potential over the period 5 h to 7 h. Optical micrographs of the crevice corroded region after an exposure period of 48 h are shown in Figure 12. The optical micrograph in Figure 12(a) shows the sharp boundary between the noncreviced and creviced regions. In the creviced region, many deep and connected pits are observed on the grain boundaries and smaller less developed pits on the individual grain surfaces (Figure 12[b]).

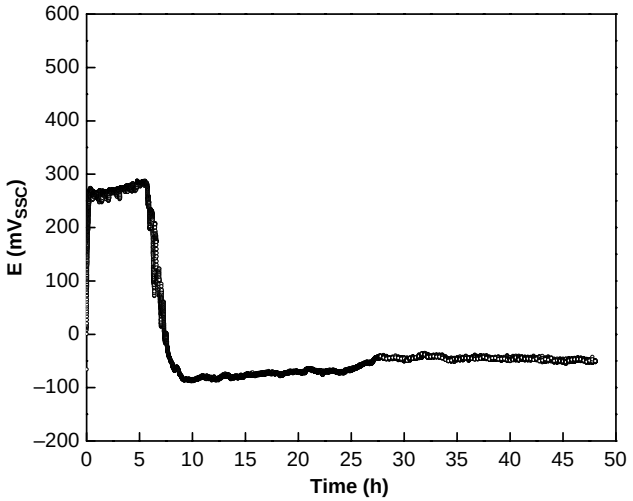

FIGURE 11. *Potential-time curve recorded on UNS N06022 at an applied current of 20 μA in 1 M NaCl (105°C) using the single crevice arrangement.*

As observed in Figures 12(a) and (b), not all of the grain boundaries in the heavily corroded region suffered intergranular corrosion. This is consistent with the observations of Jakupi, et al.,[14] who showed that, on UNS N06022, localized corrosion preferentially initiated at triple points and non-Σ3 grain boundaries. The observations of Jakupi, et al., were on more lightly crevice corroded specimens in experiments conducted at a lower temperature (70°C). At the higher temperature of 105°C used in this study, pit growth is more rapid and grain boundary selectivity less marked.

Figure 13 shows an SEM image of a creviced corroded region on UNS N06022 near the crevice edge and a series of EDX maps for the various alloy constituents. The interlinked pits along the grain boundaries contain corrosion product deposits, enriched in Mo, W, and O and depleted in Ni and Cr, consistent with previous observations,[12,15] indicating that pit propagation is controlled by the deposition of Mo and W as a result of the local acidity arising at these active locations. Jakupi, et al.,[12] used Raman spectroscopy to show that Mo and W form as polymeric molybdates and tungstates in crevice corroded locations on UNS N06022. If it is accepted that 20% HCl is a reasonable surrogate for the critical crevice solution existing within the active locations within the crevice, then the accumulation of Mo, in the form of molybdates, would be expected at these active pit locations. As the corrosion rate should then be decreased, corrosion penetration at these locations should be limited.

To examine whether this was the case, the crevice corrosion damage sustained on UNS N06625 (9 wt% Mo) and UNS N06059 (16 wt% Mo) was compared, as both have similar Cr contents and neither alloy contains W (Table 1). Figure 14 shows the 3D images of the crevice corroded region, obtained by profilometry, on both alloys after a crevice corrosion experiment. The specimens examined were from previous PD-GS-PD experiments performed in 1 M NaCl at 80°C using the MCA.[7] Visually, the depth of penetration appears considerably greater on UNS N06625 than on UNS N06059. Line scans performed on the two alloys confirm that the maximum depth of penetration is greater on UNS N06625 (~30 μm to 35 μm) compared to UNS N06059 (~2.5 μm to 3 μm).[16] These results are consistent with those of Kehler and Scully,[17] who used confocal laser scanning microscopy to show that the depth of penetration resulting from crevice corrosion was higher for UNS N06625 than for UNS N06022 (13 wt% Mo + 3 wt% W, Table 1), and confirm the role of Mo in suppressing alloy corrosion under active highly acidic conditions. Additionally, inspection of the profiles and line scans[16] show that corrosion damage is uniformly distributed around the mouth of the crevice on UNS N06059, but highly localized at one edge on UNS N06625.

As these experiments were conducted under constant current conditions, propagation is supported

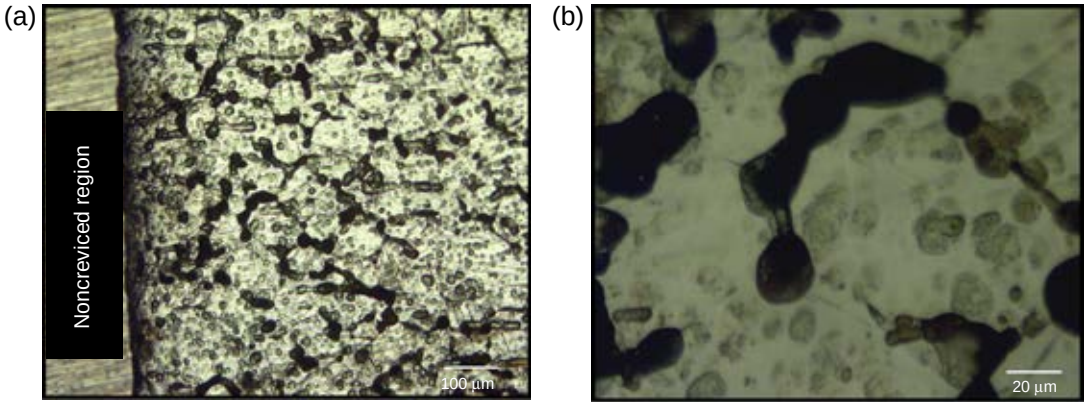

FIGURE 12. *Optical micrographs of the crevice corroded region on UNS N06022 at different magnifications after the experiment described in Figure 11: (a) 100× and (b) 500×.*

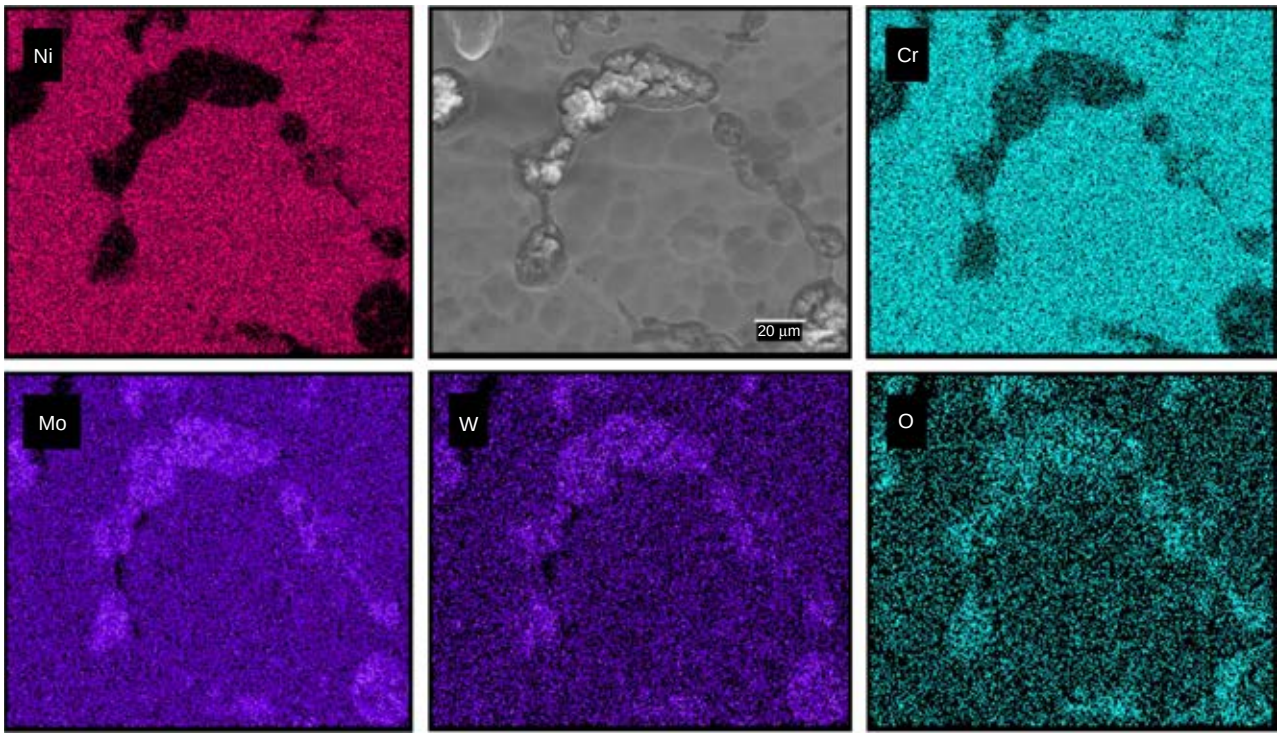

FIGURE 13. *SEM micrograph and EDX maps of the crevice corroded region on UNS N06022 showing the Mo/W/O corrosion product deposits formed on the grain boundaries.*

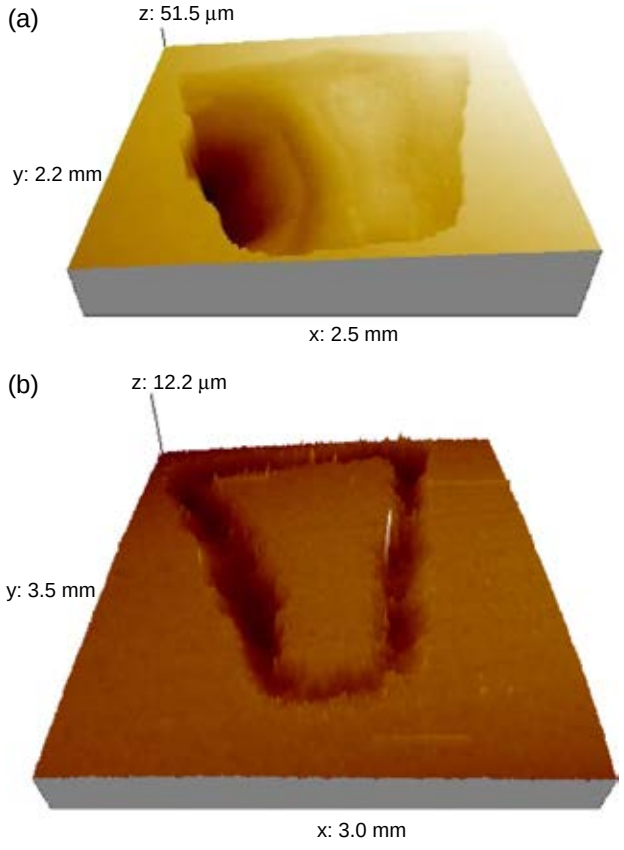

FIGURE 14. *3D images of the creviced corroded regions on (a) UNS N06625 and (b) UNS N06059 obtained by profilometry after PD-GS-PD experiments at 80°C in 1.0 mol/L NaCl.*

and repassivation prevented. Under these conditions, enforced propagation penetrates deep into UNS N06625 at the location at which crevice corrosion initiates, as the Mo content is too low to build up the molybdate deposits required to prevent it. By contrast, on UNS N06059 penetration is limited by the accumulation of molybdates at the initiation site, forcing propagation to proceed laterally around the outer edge of the crevice. These observations are consistent with those of Jakupi, et al.,[18] who showed that the depth of penetration of crevice corrosion on UNS N06022 was dependent on the current applied, the rate of molybdate formation increasing at higher currents forcing lateral propagation, and limiting the depth of propagation.

To confirm that Mo is concentrated within active locations, AES depth profiles were recorded within the creviced area on UNS N06059 (Figure 15). The profile for a corroded area (1) is shown in Figure 15(b). Generally, for AES measurements, the film thickness can be determined as the depth at which the oxygen concentration reaches half of its surface value, as this is taken to be the approximate location of the alloy/oxide interface.[19-23] Using this criterion, the thickness of the film on the surface of area 1 is >100 nm (Figure 15[b]). Although the oxide/alloy interface is difficult to locate, there is a very obvious enrichment in Mo within the corrosion product, confirming its accumulation occurs at actively corroded locations.

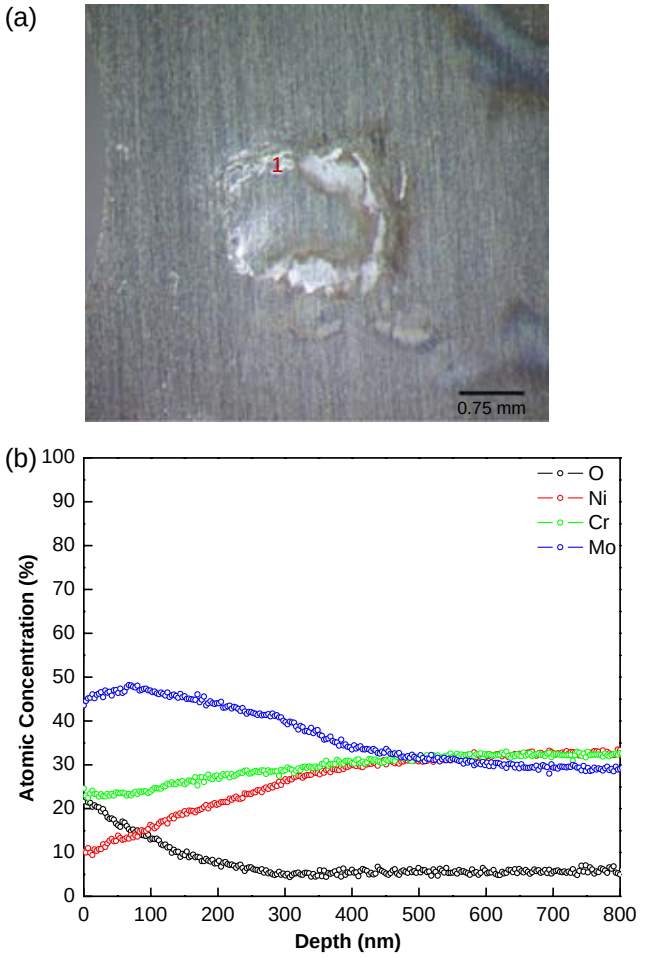

FIGURE 15. *(a) Optical image of a crevice corroded region on UNS N06059 and (b) an AES depth profile recorded at location 1 in (a).*

CONCLUSIONS

❖ Ni-based alloys containing high Mo (like UNS N10675 and N10362) demonstrate the highest corrosion resistance in reagent grade concentrated HCl solutions. In the presence of moderate to high levels of oxidizing impurity (Fe^{3+}), an alloy with a high Cr content (e.g., UNS N06200 and N06022) is required in order to maintain a low corrosion rate.

❖ Under natural conditions, the surface oxide that provides protection against corrosion in concentrated HCl is enriched in Mo.

❖ The distribution and extent of crevice corrosion damage depends strongly on the Mo (Mo + W) content of the alloy.

❖ On alloys containing only a small Mo (Mo + W) content (e.g., UNS N06625 [9Mo]), the crevice propagation penetrates deep into the alloy at the initiation site.

❖ On an alloy with a higher Mo (Mo + W) content (e.g., UNS N06022 [13Mo + 3W]), propagation occurred as a series of interlinked shallow pits along grain boundaries, with the depth of penetration in any individual pit being limited by the accumulation of molybdates and tungstates.

ACKNOWLEDGMENTS

The authors greatly acknowledge the support from Surface Science Western (SSW) at Western University, Canada for surface characterization. Also, the author acknowledges the efforts of corrosion technician Ryan Markley and Jeff Dillman from Haynes International in conducting the corrosion tests.

REFERENCES

1. C.P. Dillon, W.I. Pollock, eds., *Materials Selector for Hazardous Chemicals*, Vol. 3: Hydrochloric Acid, Hydrogen Chloride and Chlorine (St. Louis, MO: Materials Technology Institute of the Chemical Process Industries, Inc., 1999).
2. P. Crook, N.S. Meck, J. Crum, R.B. Rebak, "Corrosion of Nickel and Nickel–Base Alloys," in *Corrosion: Materials*, eds. S.D. Cramer, B.S. Covino Jr., ASM Handbook, vol. 13B (Materials Park, OH: ASM International, 2005), p. 228.
3. J.R. Hayes, J.J. Gray, A.W. Szmodis, C.A. Orme, *Corrosion* 62 (2006): p. 491.
4. M. Moriya, M.B. Ives, *Corrosion* 40 (1984): p. 62.
5. M. Moriya, M.B. Ives, *Corrosion* 40 (1984): p. 105.
6. R. Qvarfort, *Corros. Sci.* 40 (1998): p. 215.
7. A.K. Mishra, D.W. Shoesmith, *Corrosion* 70 (2014): p. 721.
8. N.S. Meck, P. Crook, D.L. Klarstrom, "Effect of Ferric Ions on the Corrosion Performance of Nickel Alloys in Hydrochloric Acid Solutions," CORROSION 2004, paper no. 430 (Houston, TX: NACE International, 2004).
9. ASTM G59, "Standard Test Method for Conducting Potentiodynamic Polarization Resistance Measurements" (West Conshohocken, PA: ASTM International, 2014).
10. A.K. Mishra, X. Zhang, D.W. Shoesmith, *Corrosion* 72 (2016): p. 356.
11. A.K. Mishra, G.S. Frankel, *Corrosion* 64 (2008): p. 836.
12. P. Jakupi, F. Wang, J.J. Noel, D.W. Shoesmith, *Corros. Sci.* 53 (2011): p. 1670.
13. D.A. Jones, *Principles and Prevention of Corrosion*, 2nd ed. (Upper Saddle River, NJ: Prentice Hall, 1996).
14. P. Jakupi, J.J. Noel, D.W. Shoesmith, *Electrochem. Solid-State Lett.* 13 (2010): p. C1.
15. X. Shan, J.H. Payer, *J. Electrochem. Soc.* 156 (2009): p. C313.
16. A.K. Mishra, N. Ebrahimi, D.W. Shoesmith, P.E. Manning, "Materials Selection for Use in Hydrochloric Acid," CORROSION 2016, paper no. 7680 (Houston, TX: NACE, 2016).
17. B.A. Kehler, J.R. Scully, *Corrosion* 61 (2005): p. 665.
18. P. Jakupi, J.J. Noel, D.W. Shoesmith, *Corros. Sci.* 54 (2012): p. 260.
19. A.S. Lim, A. Atrens, *Appl. Phys. A* 54 (1992): p. 343.
20. S. Mischler, A. Vogel, H.J. Mathieu, D. Landolt, *Corros. Sci.* 32 (1991): p. 925.
21. M.G. Faichuk, S. Ramamurthy, W.M. Lau, *Corros. Sci.* 53 (2011): p. 1383.
22. A.K. Mishra, S. Ramamurthy, M. Biesinger, D.W. Shoesmith, *Electrochim. Acta* 100 (2013): p. 118.
23. A.K. Mishra, D.W. Shoesmith, *Electrochim. Acta* 102 (2013): p. 328.